Research Article

Gianluigi Zito, Gennaro Sanità, Bryan Guilcapi Alulema, Sofía N. Lara Yépez, Vittorino Lanzio, Fabrizio Riminucci, Stefano Cabrini, Maria Moccia, Concetta Avitabile, Annalisa Lamberti, Vito Mocella, Ivo Rendina and Silvia Romano*

Label-free DNA biosensing by topological light confinement

https://doi.org/10.1515/nanoph-2021-0396
Received July 22, 2021; accepted October 13, 2021;
published online November 10, 2021

Abstract: Large-area and transparent all-dielectric metasurfaces sustaining photonic bound states in the continuum (BICs) provide a set of fundamental advantages for ultrasensitive biosensing. BICs bridge the gap of large effective mode volume with large experimental quality factor. Relying on the transduction mechanism of reactive sensing principle, herein, we first numerically study the potential of subwavelength confinement driven by topological decoupling from free space radiation for BIC-based biosensing. Then, we experimentally combine this capability with minimal and low-cost optical setup, applying the devised quasi-BIC resonator for PNA/DNA selective biosensing with real-time monitoring of the binding event. A sensitivity of 20 molecules per micron squared is achieved, *i.e.* ≃0.01 pg. Further enhancement can easily be envisaged, pointing out the possibility of single-molecule regime. This work aims at a precise and ultrasensitive approach for developing low-cost point-of-care tools suitable for routine disease prescreening analyses in laboratory, also adaptable to industrial production control.

Keywords: biosensors; bound states in the continuum; DNA; photonic crystals.

1 Introduction

Advanced biomedical diagnostic technologies play a key role in improving healthcare and clinical diagnostic processes. Optical chemical and biological sensors are at the forefront of this advancement as they offer high sensitivity, label-free monitoring, and simultaneous detection of multiple biomarkers. The possibility of engineering high quality factor cavities in microsphere resonators, ring resonators, photonic crystal resonators, waveguides, and circuits has led to interesting applications for perturbation-type measurements used in ultrasensitive (single molecule) biosensing. In this direction, also photonic crystal slabs (PhCS) and metasurfaces sustaining bound states in the continuum (BICs) were investigated [1], demonstrating the capability of highly sensitive trace-detection down to few-molecules regime [2–8], with potential electrical tunability [9]. In strict analogy with whispering gallery modes and PhCS defect-nanocavity resonators, the physical transduction mechanism which the quasi-BIC resonator depends on is based on reactive sensing principle [10].

In this work, we show that – despite the delocalized nature of the field in the transverse plane – our PhCS is capable of a sensitivity of few-molecules per micron squared of sensing area even in realistic experimental settings in which the resonance quality factor becomes $Q \sim 10^2$. In particular, this is directly associated to the deep subwavelength optical field confinement in the slab having a thickness of only 50 nm. We apply our quasi-BIC resonator to design a general biosensing system. Biosensors based on synthetic oligonucleotides such as peptide nucleic acids (PNAs) have provided an alternative to conventional platforms, pushing down the selectivity, and the sensitivity of nucleic acid assay [11]. Herein, we use a suitable PNA

Gianluigi Zito and **Gennaro Sanità** equally contributed to this paper.

***Corresponding author: Silvia Romano**, Institute of Applied Sciences and Intelligent Systems, National Research Council, Naples, Italy, E-mail: silvia.romano@cnr.it. https://orcid.org/0000-0002-8432-7611
Gianluigi Zito, **Gennaro Sanità**, **Bryan Guilcapi Alulema**, **Sofía N. Lara Yépez**, **Vito Mocella and Ivo Rendina**, Institute of Applied Sciences and Intelligent Systems, National Research Council, Naples, Italy, E-mail: gianluigi.zito@na.isasi.cnr.it (G. Zito). https://orcid.org/0000-0003-2376-0080 (G. Zito)
Vittorino Lanzio, **Fabrizio Riminucci and Stefano Cabrini**, Molecular Foundry, Lawrence Berkeley National Laboratory, Berkeley, CA, USA
Maria Moccia and Concetta Avitabile, Institute of Crystallography, National Research Council, Bari, Italy
Annalisa Lamberti, Department of Molecular Medicine and Medical Biotechnology, University of Naples Federico II, Naples, Italy

sequence immobilized on the PhCS to selectively target DNA molecules of interest. This approach represents a proof of principle for biosensor settings in which ultrasensitive and selective optical detection can be based on PNA/DNA recognition, such as for trace analysis of liquid-biopsy biomarkers of various pathologies, associated as for instance to diabetes or cancers.

2 Optical transduction mechanism

The photonic BIC, thus far studied in several systems [12–19], is a topological singular point in the reciprocal space [16, 20]. It is the core of the polarization vortex of the leaky radiation having momentum progressively closer to the BIC point, at which polarization becomes undefined. This disengages the mode from radiation loss, virtually increasing its lifetime indefinitely, and as such also its radiative Q-factor. This can induce a large near field localization [21] that was used in many applications, many of them reviewed in [22], and also more exotic phenomena like spin-directive coupling of light [23]. The high Q-factor is interesting because can act balancing the large effective mode volume V_{eff} of the all-dielectric nanostructure resonance, thus inducing a large ratio Q/V_{eff}, that ultimately defines the metrics for nanoscale enhancement.

Despite being in the light cone, the BICs have experimentally Q-factor much larger than the guided modes (one or more orders of magnitude). This occurs because they are topologically incompatible with radiation, thus more robust against perturbation causing leaky light. In the literature, the largest experimental Q-factor in high index material is of the order of 10^5 [24], but it must be said that the Q-factor also depends on the environment. As for instance, a film of material on the PhCS will lower the Q-factor, as it occurs for microsphere resonators. Thus, we could say that an upper bound for realistic settings is 10^5 with high index materials like silicon. In transparent silicon nitride, we have observed total Q-factor of the order of 10^3 [25]. We showed the potential for ultralow weight molecular sensing [3] and trace-detection towards single molecule regime with a PhCS [8], and detailed the exponential character of its bulk refractometric sensitivity [4] and explored a correlative microscopy scheme for enhanced imaging [2]. Single-molecule regime was also put forward for quasi-BICs extruded metasurfaces in the IR range [7]. In this section, we will address the physical transduction mechanism responsible for this large spectral sensitivity.

The local optical field confined in the photonic nanostructure near the BIC point in the reciprocal space (so as matching critical coupling condition) is enhanced and has a significant energy fraction in the evanescent tail superimposed with the molecular probe. In Figure 1a, we show the numerically calculated displacement field intensity $|\boldsymbol{D}|^2$ of an accidental BIC sustained by the PhCS designed in this work (see Section 3 and Figure 3b for details on geometry). In particular, we introduced a homogeneous 10 nm biofilm of index $n_{\text{c}} = 1.55$ on top of the PhCS surface. The biofilm mimics a biological perturbation adsorbed on the PhCS when this last is placed in a certain liquid environment with refractive index $n_{\text{le}} = 1.33$ (le, liquid environment). The slab had $n_{\text{s}} = 2.15$ and is coated over a quartz slide of thickness 120 μm with refractive index $n_{\text{b}} = 1.45$.

For reactive sensing principle [10], the molecular probe in the near-field of the resonance alters the mode energy, shifting the resonance frequency and wavelength λ_{r}. In accordance with refs. [26, 27], the energy variation of resonant photons at the particle probe position $\boldsymbol{r}_{\text{o}}$ is

$$\hbar\Delta\omega_{\text{r}} \simeq -\frac{\alpha_{\text{ex}}}{2}\langle E(\boldsymbol{r}_{\text{o}}, t)\rangle^2, \tag{1}$$

where α_{ex} is the excess polarizability of the particle probe experiencing a time-averaged local field $\langle E(\boldsymbol{r}_{\text{o}}, t)\rangle$. The fractional frequency shift associated to a probe molecular layer of thickness δh and density ρ_{p} can thus be written as

$$-\frac{\Delta\omega_{\text{r}}}{\omega_{\text{r}}} = \frac{\Delta\lambda_{\text{r}}}{\lambda_{\text{r}}} = \frac{\alpha_{\text{ex}}}{2\varepsilon_0}\frac{\int_{V_\rho}\rho_{\text{p}}|\boldsymbol{E}(\boldsymbol{r})|^2\mathrm{d}V}{\int_{V_{\text{res}}}\varepsilon(\boldsymbol{r})|\boldsymbol{E}(\boldsymbol{r})|^2\mathrm{d}V}, \tag{2}$$

in which the integration is intended over the volume $V_\rho = A\delta h$ occupied by the molecules and the resonator volume V_{res}. The peak resonance shift $\Delta\lambda_{\text{r}}$ is the physical quantity experimentally measured. The BIC field in the adsorption zone of the PhCS has intensity comparable with the confined mode because $h \ll \lambda_{\text{r}}$, as also visible in Figure 1a by inspecting the fraction of the evanescent tail overlapped with the biofilm. The perturbation of a photonic cavity by a material of thickness δh can be written considering that the resonance tuning will change so as satisfying cavity boundary conditions. Neglecting the local filed influence in a first approach, if the resonator has a characteristic length h (the thickness of the slab in case of our PhCS), with refractive index n_{s}, then the perturbation of the probe material of index n_{c} will affects the resonance peak such that

$$\frac{2\pi}{\lambda_{\text{r}}}n_{\text{s}}h \sim \frac{2\pi}{\lambda'_{\text{r}}}(n_{\text{s}}h + n_{\text{c}}\delta h). \tag{3}$$

Thus, we could consider that $\lambda'_{\text{r}} = \lambda_{\text{r}} + \Delta\lambda_{\text{r}}$, with

$$\frac{\Delta\lambda_{\text{r}}}{\lambda_{\text{r}}} \sim \frac{\delta h}{h}. \tag{4}$$

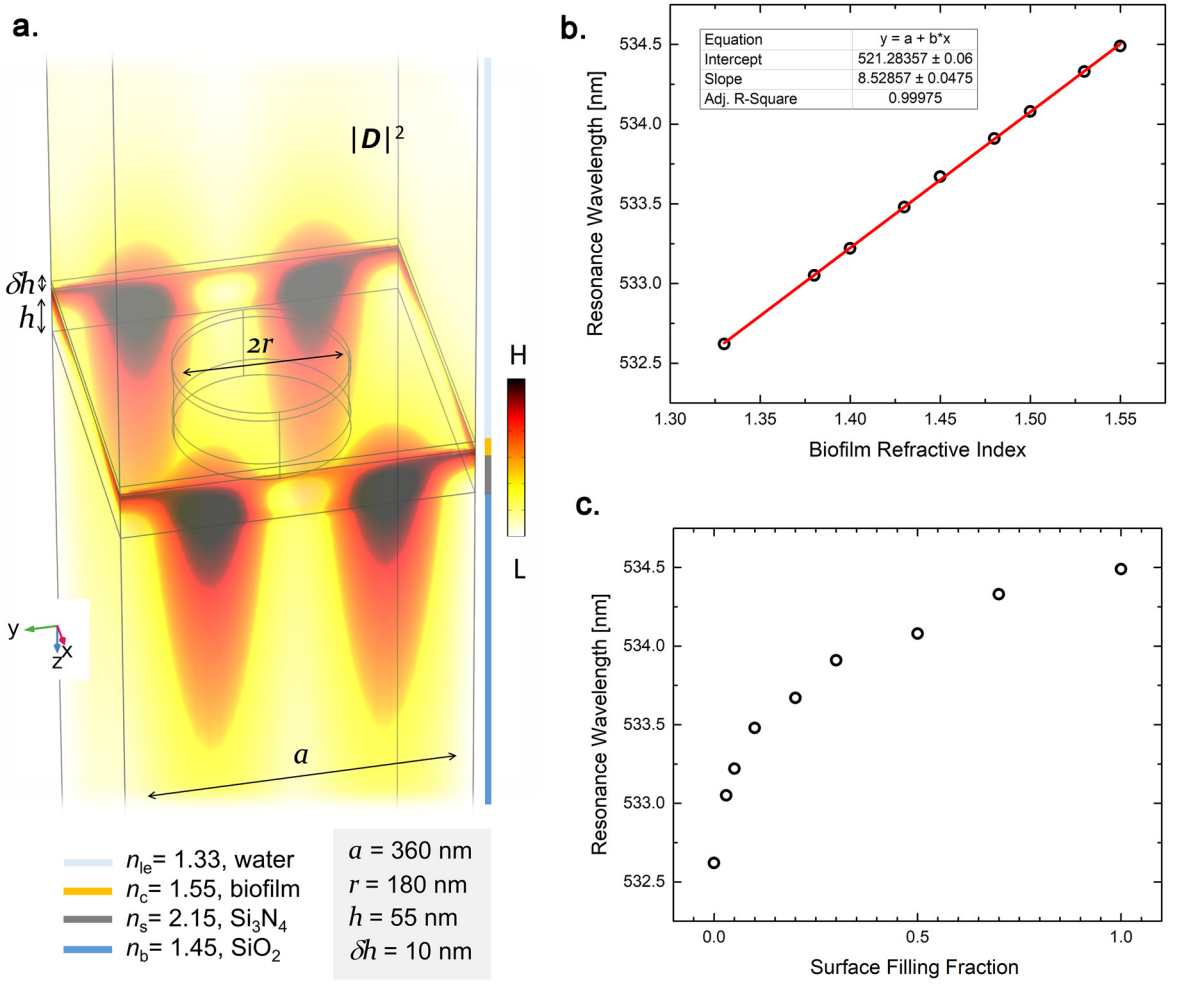

Figure 1: Simulation results.
(a) Numerically simulated displacement field of an accidental BIC in our PhCS. On top of the PhCS a 10 nm biofilm with $n_c = 1.55$ is included, soaked in liquid environment with refractive index $n_{le} = 1.33$. (b) The resonance wavelength of the BIC, λ_r, is plotted as a function of n_c, mimicking a partial-to-total homogeneous filling of the biofilm region with molecules with $n_c = 1.55$. (c) λ_r behavior traced as a function of the surface filling fraction corresponding to the plot in (b).

Indeed, we can write that

$$\int_{V_{res}} \varepsilon(\boldsymbol{r})|\boldsymbol{E}(\boldsymbol{r})|^2 \mathrm{d}V = \varepsilon(\boldsymbol{r}_{max})|\boldsymbol{E}(\boldsymbol{r}_{max})|^2 V_{eff} \doteq c_v A h, \quad (5)$$

in which we defined the volume coefficient c_v and correlated it with the effective mode volume V_{eff} ($\boldsymbol{r}_{max}$ defines the maximum of the optical field). In addition, if we take into account a homogeneous probe density ($\rho_p = \text{const}$) and neglect the field variation over the thickness $\delta h \ll \lambda_r$, we can also define a surface coefficient c_s by

$$\int_{V_\rho} \rho_p |\boldsymbol{E}(\boldsymbol{r})|^2 \mathrm{d}V = \rho_p \delta h \int_{\Sigma} |\boldsymbol{E}(\boldsymbol{r})|^2 \mathrm{d}A \doteq \rho_p c_s A \delta h. \quad (6)$$

Substituting Eqs. (5) and (6) in (2), it follows that

$$\frac{\Delta\lambda_r}{\lambda_r} = \beta(\lambda_r)\frac{\delta h}{h}, \quad (7)$$

with

$$\beta(\lambda_r) \doteq \frac{\alpha_{ex}}{2}\rho_p \frac{c_s}{c_v}. \quad (8)$$

The coefficient c_s measures the superposition of the photonic mode with the probe material, whereas the coefficient c_v measures the effective mode volume of the resonance. Equation (7) is at the core of the excellent sensing capability of the BIC resonator. Indeed, the decoupling from the continuum allows confining the radiation even within a slab thickness $h = 50$ nm, which is in stark contrast to microresonators in which total internal reflection confinement requires typically sizes of the order or $L \sim 50$ µm. Experimentally, the resonance linewidth and its figure of merit (FOM), defined as the ratio between the sensitivity and the full width at half maximum (FWHM) or Q-factor, ultimately measures the capability to follow tiny changes in the environment. Higher Q and FOM point out optical

sensors with a low limit of detection (LOD). The LOD of the optical resonator is correlated to the minimal spectral shift that can be appreciated upon molecular binding [3, 28]. It can be assumed that $\Delta\lambda_{\mathrm{LOD}} = \lambda_{\mathrm{r}}/(10Q)$ [28]. Imposing $\Delta\lambda_{\mathrm{r}} \doteq \Delta\lambda_{\mathrm{LOD}}$, it follows that

$$\beta\frac{\delta h}{h} \simeq \frac{1}{10Q}, \tag{9}$$

which can be read as an equation to determine the quality factor Q^* necessary to detect a molecular probe layer of thickness δh^* by reactive sensing principle, *i.e.*

$$Q^* \geq \frac{1}{\beta^*}\frac{h}{10\delta h^*}. \tag{10}$$

In the hypothesis of same β, we can see from the above equation that detecting a protein layer with $\delta h^* = 10$ nm on top of a resonator with $h = 50$ nm (thin PhCS) would require a much lower Q with respect to microresonators with $h = L = 50$ μm, since

$$Q^*_{\mathrm{BIC}} = (h/L)\, Q^*_L = 10^{-3} Q^*_L, \tag{11}$$

i.e. three orders of magnitude lesser than what necessary for a microresonator of comparable field intensity. In other words, with Q factors of the order of $10^2 \div 10^3$, the BIC resonating nanocavity can in principle detect ρ_{p} corresponding to filling fraction well below a protein monolayer, reaching the ultrasensitive regime down to single-molecule sensitivity. To verify this property, we calculated λ_{r} for the BIC mode of Figure 1a as a function of the biofilm refractive index n_{c}. The plot is shown in Figure 1b. The variation of n_{c} simulates a progressively growing filling of the biofilm region with molecules of interest having RI = 1.55. In other words, 1.33 is the RI of the unoccupied biofilm region and 1.55 is the RI when the region is occupied. The corresponding filling fraction is shown in Figure 1c. Interestingly, a filling fraction of only 5% provides a resonance shift of ∼0.5 nm, easily detectable even with a $Q \sim 10^2$, *i.e.* a resonance at 532 nm with FWHM of 5 nm. Therefore, even in realistic biosensing settings in which the experimental linewidth typically broadens (like in solutions or colloidal suspensions), the surface refractometric sensitivity of the system can be very large.

This capability must be reconducted to the confinement mechanism, either mode symmetry mismatch or topological singularity, that allow trapping the radiation inside a thin slab of deep subwavelength thickness. The second advantage is that this occurs while the mode is delocalized in the PhCS plane, thus providing a sensing area capable of capturing more molecules increasing the response of the system. The third advantage is that the system is rather simple, scalable, integrable in complex transdisciplinary setups, and requires facile interrogation setup for microfluidics experiments with far field excitation source near to normal incidence.

3 Experimental DNA biosensing

We studied the quasi-BIC spectral resonance shift $\Delta\lambda_{\mathrm{r}}$ in a system consisted of (i) a PhCS with suitable lattice geometry for visible excitation with $h \sim \lambda_{\mathrm{r}}/10$; (ii) a passivated functional layer with single-strand PNA (ssPNA) active receptors immobilized on top of the PhCS surface; and (iii) a microfluidic chamber with top transparent glass window aligned to the PhCS. Therefore, the liquid injection brings ssDNA molecules in a PBS solution to fill the volume of the well, at the bottom of which the PhCS sensing area of 1 mm^2 is placed. The liquid environment with $n_{\mathrm{le}} \simeq 1.33$ and immobilized layer of ssPNA are the starting condition. The perturbation to the quasi-BIC mode was only provided by complementary ssDNA (c-DNA) molecules binding to PNA.

The PhCS consisted of holey square lattices inscribed in a silicon nitride (Si_3N_4) film deposited over fused silica [2], totally transparent to visible radiation for facile interrogation and transmission experiments. The geometry (lattice constant, hole radius, slab thickness), respectively (a, r, h), were optimized to realize PhCSs resonant in the visible range according to iterating numerical simulations, ellipsometric measurements of the RI dispersion of silicon nitride and experimental characterization of the pattern morphology by atomic force microscopy (Materials and Methods). The designed values reported in Figure 1a were coincident with the experimental ones except for a and r that were slightly reduced of ca. 1%.

To assess selectivity of biodetection of target DNA with PNA, two parallel PhCSs were devised, in which the negative control was injected with noncomplementary DNA (nc-DNA). The ssPNA molecules were synthesized by Fmoc chemistry (protocol is reported in [29]) and properly bound to the PhCS surface by means of a custom functionalization protocol (Figure 2a), as detailed in Materials and Methods. The ssPNA used in this work has a nucleobases sequence complementary to the miR-126, a well-known biomarker of diagnostic relevance [11]. To evaluate the binding between the ssPNA and c-DNA and confirming the absence of interaction with nc-DNA, electrophoresis mobility shift assay (EMSA) was performed [30]. 0.25 nmol of ssPNA and of fluorescent c-DNA* or nc-DNA* were incubated in 10 μL of PBS 1× at RT for 60′. The samples were then resolved by electrophoresis (20% polyacrylamide gel in Tris-acetate EDTA

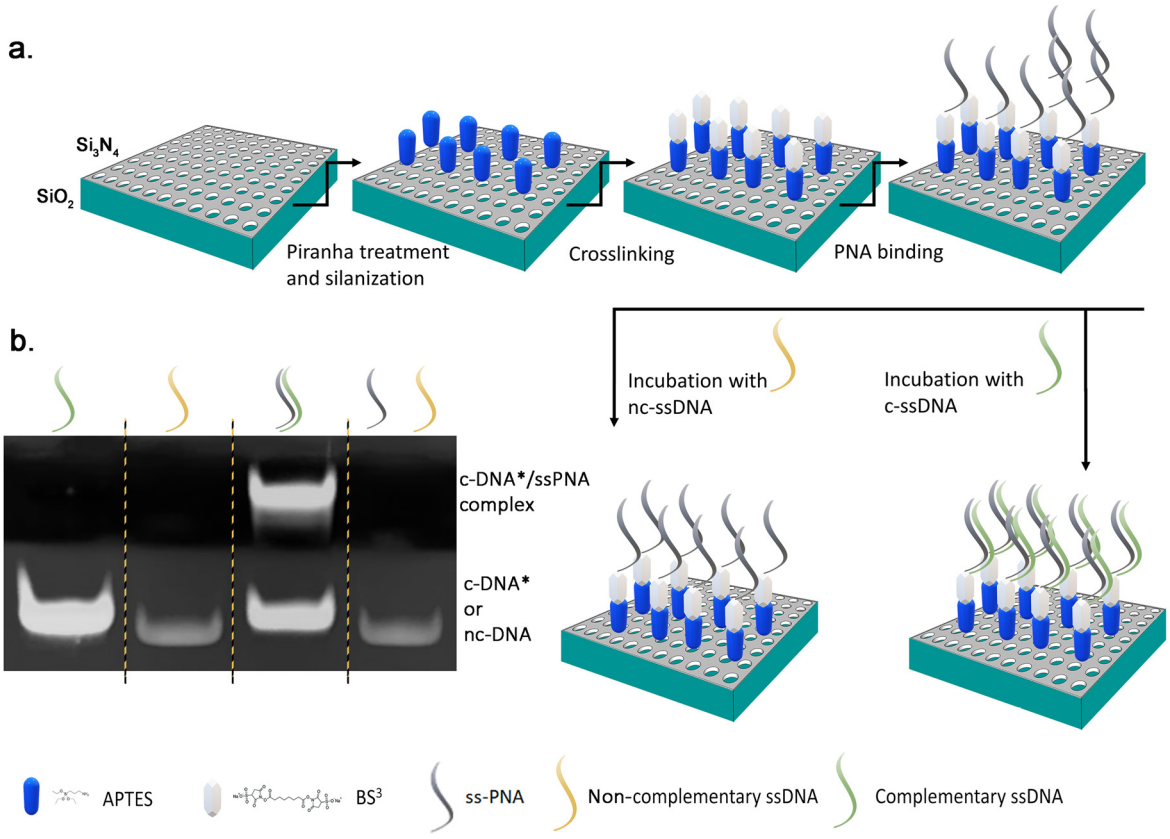

Figure 2: Functionalization protocol scheme.
(a) Functionalization approach exploited on silicon nitride surface to bind PNA bioprobes before the DNA incubation. (b) EMSA of fluorescent c-DNA* and nc-DNA* incubated with ssPNA.

buffer, at 100 V for 45′) and the DNA* was revealed by a fluorescent lamp. Figure 2b clearly shows that the interaction between PNA and c-DNA produced a complex c-DNA/PNA migrating more slowly than the corresponding free nucleic acid. No variation in the electrophoretic mobility of nc-DNA* was visible when incubated with ssPNA compared to the nc-DNA* alone. These data clearly indicate that the nc-DNA* cannot introduce possible aspecific results since it does not bind to ssPNA.

In order to examine the spectral position and the origin of different types of modes, the PhCS band diagram was experimentally reconstructed. Figure 3 shows the experimental PhCS band diagrams measured in air and PBS after functionalization. Transmission spectra were acquired in a suitable angular range with motorized rotational stage and step of 0.01° with a custom-built Matlab routine. Three relevant dispersion bands were observed. While the lower energy mode with vanishing linewidth towards the high symmetric point at normal incidence is a symmetry-protected BIC, other two Friederich–Wintgen accidental BICs appear in the photonic system when $n_{le} = 1.33$. The mode profile of the resonance at ~532 nm at ~3° was shown in Figure 1a. Preliminary tests pointed out that the resonance broadening and intensity upon molecular binding was minimally affected at this angle, while the spectral shift was significant as signature of large local near-field. Therefore, we set the incidence angle to ~3° to trace the BIC evolution upon DNA binding. Figure 4a shows a sketch of the device. A short-wavelength pass filter was used to avoid IR absorption since the supercontinuum light source had a spectrum going from 450 to 2100 nm. One of the chambers was initially filled with PBS to establish a baseline in the acquired transmittance. The transmittance spectrum at the selected angle was then acquired as a function of the incubation time with c-DNA or nc-DNA. The quasi BIC resonant peak, analyzed monitoring the spectral centroid and Fano peak fit with Matlab, is shown in Figure 4b as a function of the incubation time, after injecting a total volume of 60 µL. After the plateau reached with c-DNA at 0.1 nM in PBS, a second concentration of 0.25 nM was injected. The evolution curves showed a good responsiveness of the device even with a minimal concentration of 0.05 nM of c-DNA (Figure 4b, inset). This concentration value in a volume of 60 µL corresponded to 1.8×10^9 c-DNA

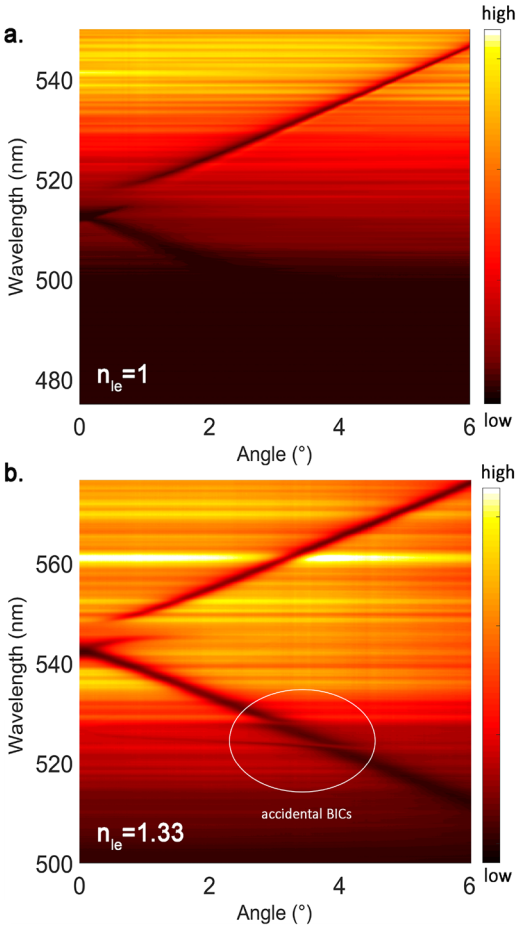

Figure 3: Band diagrams.
(a) Experimental dispersion diagrams along ΓX of the PhCS for n_{le} = 1 (air) and (b) $n_{le} = 1.33$ (PBS). High-Q resonances are generated by Friederich–Wintgen (accidental) BICs between 3 and 4° when the solution is present on top of the PhCS: their spectral shift is monitored as a function of the DNA binding.

molecules. The bottom area of the chamber was homogeneously covered with ssPNA and had a diameter of 6 mm with a central square sensing area of 1 mm of side, *i.e.*, ∼3% of the available surface. At 0.05 nM, the maximum number of molecules capable of binding to the surface was easily estimated to be <20 molecules/μm^2, value that corresponded to a total DNA weight on the PhCS area of p = 11 fg = 0.011 pg. Figure 4c (left-panel) shows the full transmittance spectra before and after incubation with c-DNA (C = 0.1 nM). After the incubation time, the surface was washed by PBS solution and water to remove any aspecific bindings, confirming the spectral shift monitored during the incubation. The spectral shift was then measured at various concentrations of c-DNA and the resulting average value is shown in Figure 4c (right-panel).

The near field enhancement and hence the fraction of energy density superimposed with the material to detect must be maximized to have a good spectral sensitivity. Reciprocity implies that the maximum local field enhancement is reached at the critical coupling condition [31], not at the BIC point because there would be too poor coupling. The critical coupling condition for the accidental BIC in Figure 3b is in between the BIC point and the band-edge state at normal incidence, thus maximizing the local field close to 3°. Experimentally, it is very easy to follow its spectral evolution upon surface adsorption measurements. In contrast, the critical coupling condition of the symmetry-protected BIC occurs at arbitrary angles of incidence, up to 10–20°, which makes a stable and long-term interrogation system far trickier. As a matter of fact, by inspecting Figure 4c, it is possible to observe that the shift of the first resonance (accidental BIC) is a factor 2.5 larger than the fourth resonance (symmetry-protected BIC), and so does the refractometric surface sensitivity because of larger light–matter superposition. It is worth mentioning however that for large-scope bulk RI sensing, the accidental BIC is not an always the best choice, since it exists only a certain refractometric window of the liquid environment close to n_{le} = 1.33, which must be tailored on the application, as we also showed in our previous work [2].

The LOD is determined at a first order by the capability to detect a spectral variation of the resonance peak, and it is basically described in our previous paper and references therein [3]. In this specific experiment, as it can be seen in the inset of Figure 4b for the concentration of 0.05 nM, actually the LOD can be inferred by taking into account the spectral fluctuation of the peak as a function of the binding time. The analysis of this statistical fluctuation allowed us to estimate a- LOD of 10 pM (i.e. 2.2 fg) as the minimal quantity that our system could appreciate given the readout noise (peak fluctuation).

One important limitation of our PNA/DNA sensing scheme is that since a selective targeting is desired, the PNA layer required for this task already shifts the resonance, and as such any further shift induced by DNA is in part limited.

For what concerns reproducibility of the measurements, we applied the sensing platform repeatedly observing a stable performance. Once characterized the band diagram of PhCS, the behavior is easily predictable and reproducible. In addition, the platform can also be regenerated by standard cleansing protocols to remove organic or inorganic adsorbed materials a few times.

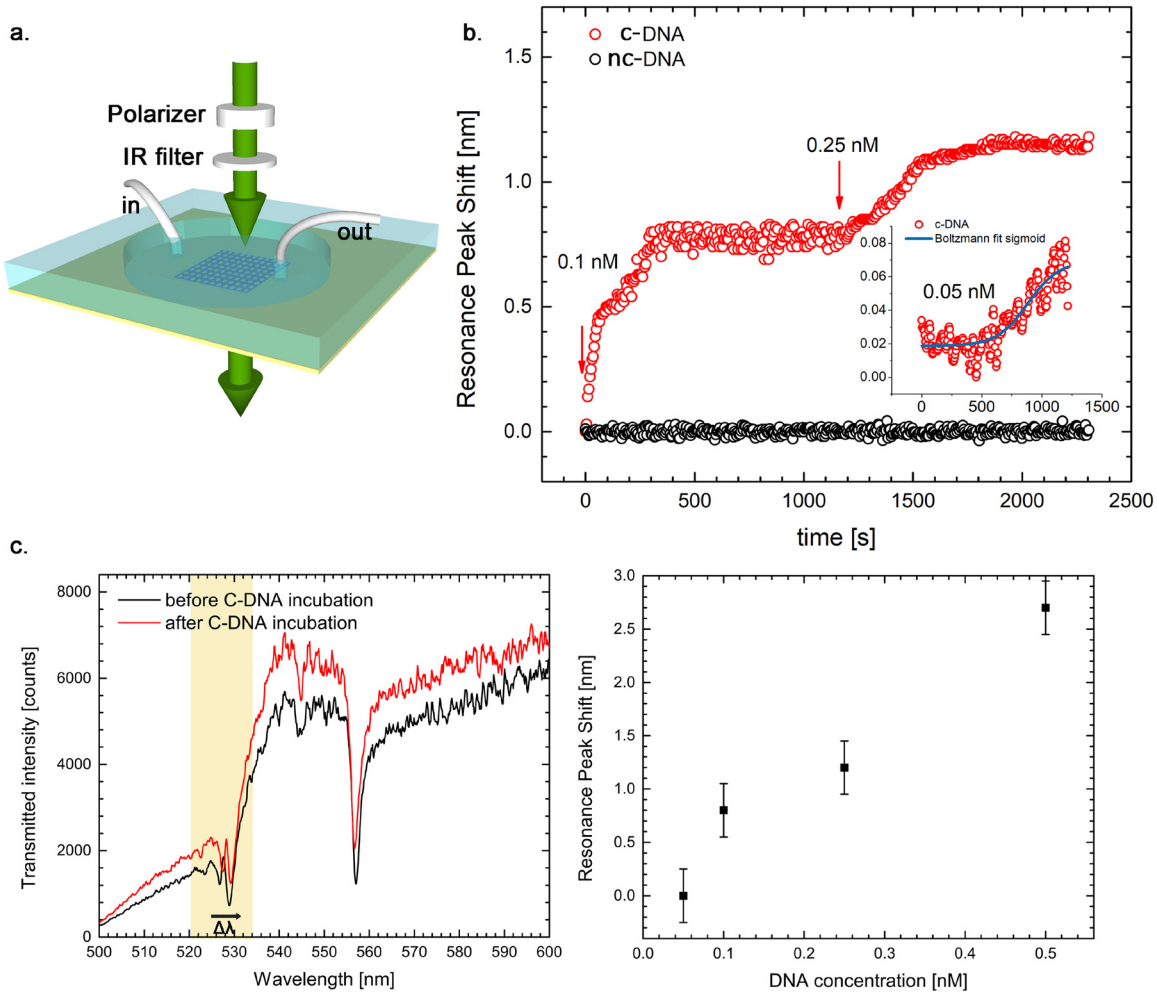

Figure 4: Experimental results.
(a) Schematic layout of the PhCS integrated in the microfluidic chamber and basic characterization setup (input light is polarized with a Glan–Thompson polarizer and the IR component is attenuated with a filter). (b) Binding assay conducted in PBS showing the shift in resonance position against time with each concentration of DNA. (c) Left: Representative resonance spectra in refractometric sensing before and after the c-DNA incubation ($C = 0.1$ nM). Right: Resonance peak wavelength as a function of the c-DNA·PNA complex.

4 Conclusions

In this work, we showed the potential of light confinement in a deep subwavelength photonic resonator sustaining Friederich–Wintgen bound states in continuum for ultrasensitive biosensing with facile interrogation and low-cost optical setup. Numerical simulations, supported by experimental characterizations, pointed out the capability of a BIC resonator to provide large surface binding sensitivity with a label-free spectral readout. Proper peptidic nucleic acids were immobilized on the photonic crystal slab. Our device was finally tested in a microfluidic well to respond by complementary DNA binding with excellent sensitivity, demonstrating the capability of detecting concentrations down to ~0.05 nM (0.011 pg). It is worth mentioning that nucleic acids (DNA, RNA and microRNA) are relevant biomarkers of several pathologies and disease conditions. The sensitive architecture developed in this work holds promise to devise a point-of-care platform based on oligomers that can find a variety of diagnostic and therapeutic applications for fast and low-cost routine analyses.

5 Materials and methods

5.1 Numerical simulations

Numerical simulations of the PhCS reflectance spectra were carried out by using a full three-dimensional rigorous coupled wave approach (RCWA) based on a Fourier modal expansion. Additional

finite element method-based simulations, carried out with Comsol Multiphysics 5.2a, were used to verify the numerical results. Bloch periodic boundary condition to surfaces along x-, y-directions was used. On top and bottom surfaces, normal to the z-direction, perfectly-matched-layer absorbing boundary conditions were used [32, 33]. The adapted mesh along z had a size-step of 3 nm inside the PhCS and increased outside, up to a value of 20 nm.

5.2 Fabrication

The PhCS in Si_3N_4 was patterned by means of electron beam lithography and reactive ion etching process. The Si_3N_4 film was deposited by plasma enhanced chemical vapor deposition (PECVD) on quartz substrate. For details see [3].

5.3 Optical characterization

Angular-resolved measurements allowed us to reconstruct the dispersion diagrams of the PhCS (including the functionalization and biosensor layer detailed below), acquiring the transmitted signal $T(\lambda, \theta)$ as a function of the input angle θ.

5.4 Surface functionalization protocol

Before starting the functionalization, PhCSs were cleaned through three washes with absolute ethanol, and three with double stilled water (ddH_2O) for 5′ at room temperature (RT). In order to introduce silanol groups (Si-OH) on silicon nitride surface, the crystals were immersed in hexane (5′ at RT), in ddH2O (5′ at RT) and in piranha solution (H_2SO_4:H_2O_2 3:1 v/v) for 60′ at 90 °C. Then, sequential immersions in aqueous solutions NaOH 0.5 M (20′ at RT), HCl 0.1 M (10′ at RT), NaOH 0.5 M (10′ at RT), HCl 0.1 M (5′ at RT) were performed. Finally, the PhCSs were washed with (ddH_2O) (5′ at RT). To introduce amino groups ($-NH_2$) through silanization, the surfaces were dried under N_2 flux and immersed in APTES (3-aminopropyltriethoxysilane) solution (5% v/v in anhydrous toluene) for 120′ at 37 °C. Next, the crystals were washed three times with toluene (2′ at RT) and heated at 100 °C for 10′ (curing). The PhCSs was then functionalized with BS_3 (bis(sulfosuccinimidyl)suberate), an amino reactive crosslinker. To this aim, the crystals was covered with 10 mM BS_3 in 20 mM HEPES buffer pH 8.3 for 5 h at 4 °C, washed three times with 20 mM HEPES buffer pH 8.3 and three times with (ddH_2O) (5′ at RT), and dried under N_2 flux. The final modification of the PhCSs was performed to bind covalently the NH_2 modified ssPNA. To this aim, the BS3 modified PhCSs were incubated with ssPNA-NH_2 300 μM in HEPES 20 mM pH 8.3 at 4 °C overnight. Next, the surface was washed three times with HEPES 20 mM pH 8.3 (5′ at RT) and three times with ddH_2O (5′ at RT). To saturate the N-hydroxysuccinimide ester (NHS) groups of BS_3 molecules that have not reacted with ssPNA-NH_2, the PhCSs were incubated with TRIS-HCl 100 mM, pH 7.4 per 30′ at RT. Finally, the PhCSs were washed with PBS 1× for three times for 5′ at RT.

5.5 PNA bioprobes synthesis

For the synthesis of PNA, Fmoc-PAL-PEG-PS resin supplied by Applied Biosystem was used [29]. The HOBT activators and HBTU were purchased from Novabiochem, while piperidine, DIPEA, acetic anhydride, and TFA were purchased from Biosolve. The N-methylmorpholine and rhodamine isothiocyanate were purchased from Sigma-Aldrich company. The anhydrous solvents for the synthesis of PNAs (DCM, DMF) were provided by the J.T. Baker company. Fmoc-PNA-cytosine (Bhoc)-OH, Fmoc-PNA-thymine-OH, Fmoc-PNA-guanine-(Bhoc)-OH, Fmoc-PNA-adenine-(Bhoc)-OH were provided by Panagene. Analytical analyses and purification of PNA oligomers were performed on HPLC equipped with UV detector and autosampler, Agilent 1100 Hewlett Packard. The synthesis consists of repetitive cycles of deprotection, coupling and acetylation, at room temperature. To improve the efficiency of the coupling reaction, double couplings were performed on G and A monomers.

Acknowledgment: We are thankful to Scott Dhuey, Molecular Foundry, Lawrence Berkeley National Laboratory, USA, for assistance in fabrication process.

Author contribution: All the authors have accepted responsibility for the entire content of this submitted manuscript and approved submission.

Research funding: Financial support from projects ARS01-01270 IDF-SHARID PON 2014-2020 and PIT-STOP grant no. PRIN-2017-20173CRP3H, MIUR, Italy is acknowledged. Work at the Molecular Foundry was supported by the Office of Science, Office of Basic Energy Sciences, of the U.S. Department of Energy under Contract No. DE-AC02-05CH11231.

Conflict of interest statement: The authors declare no conflicts of interest regarding this article.

References

[1] C. W. Hsu, B. Zhen, A. D. Stone, J. D. Joannopoulos, and M. Soljacic, "Bound states in the continuum," *Nat. Rev. Mater.*, vol. 1, no. 9, pp. 1–13, 2016.

[2] S. Romano, M. Mangini, E. Penzo, et al., "Ultrasensitive surface refractive index imaging based on quasi-bound states in the continuum," *ACS Nano*, vol. 14, no. 11, pp. 15417–15427, 2020.

[3] S. Romano, G. Zito, S. Torino, et al., "Label-free sensing of ultralow-weight molecules with all-dielectric metasurfaces supporting bound states in the continuum," *Photon. Res.*, vol. 6, no. 7, pp. 726–733, 2018.

[4] S. Romano, G. Zito, S. N. L. Yépez, et al., "Tuning the exponential sensitivity of a bound-state-in-continuum optical sensor," *Opt. Express*, vol. 27, no. 13, pp. 18776–18786, 2019.

[5] D. N. Maksimov, V. S. Gerasimov, S. Romano, and S. P. Polyutov, "Refractive index sensing with optical bound states in the continuum," *Opt. Express*, vol. 28, no. 26, pp. 38907–38916, 2020.

[6] Y. Liu, W. Zhou, and Y. Sun, "Optical refractive index sensing based on high-Q bound states in the continuum in free-space coupled photonic crystal slabs," *Sensors*, vol. 17, no. 8, p. 1861, 2017.

[7] F. Yesilkoy, E. R. Arvelo, Y. Jahani, et al., "Ultrasensitive hyperspectral imaging and biodetection enabled by dielectric

metasurfaces,'' *Nat. Photonics*, vol. 13, no. 6, pp. 390–396, 2019.
[8] S. Romano, A. Lamberti, M. Masullo, et al., ''Optical biosensors based on photonic crystals supporting bound states in the continuum,'' *Materials*, vol. 11, no. 4, pp. 1–11, 2018.
[9] E. Penzo, S. Romano, Y. Wang, et al., ''Patterning of electrically tunable light-emitting photonic structures demonstrating bound states in the continuum,'' *J. Vac. Sci. Technol., B: Nanotechnol. Microelectron.: Mater., Process., Meas., Phenom.*, vol. 35, no. 6, p. 06G401, 2017.
[10] F. Vollmer, S. Arnold, and D. Keng, ''Single virus detection from the reactive shift of a whispering-gallery mode,'' *Proc. Natl. Acad. Sci. U. S. A.*, vol. 105, no. 52, pp. 20701–20704, 2008.
[11] R. D'Agata, M. C. Giuffrida, and G. Spoto, ''Peptide nucleic acid-based biosensors for cancer diagnosis,'' *Molecules*, vol. 22, no. 11, p. 1951, 2017.
[12] E. N. Bulgakov and A. F. Sadreev, ''Bound states in the continuum in photonic waveguides inspired by defects,'' *Phys. Rev. B: Condens. Matter Mater. Phys.*, vol. 78, no. August, p. 0751051, 2008.
[13] Y. Plotnik, O. Peleg, F. Dreisow, et al., ''Experimental observation of optical bound states in the continuum,'' *Phys. Rev. Lett.*, vol. 107, no. 18, p. 183901, 2011.
[14] M. I. Molina, A. E. Miroshnichenko, and Y. S. Kivshar, ''Surface bound states in the continuum,'' *Phys. Rev. Lett.*, vol. 108, no. February, p. 0704011, 2012.
[15] C. W. Hsu, B. Zhen, J. Lee, et al., ''Observation of trapped light within the radiation continuum,'' *Nature*, vol. 499, no. 7457, pp. 188–191, 2013.
[16] B. Zhen, C. W. Hsu, L. Lu, A. D. Stone, and M. Soljačić, ''Topological nature of optical bound states in the continuum,'' *Phys. Rev. Lett.*, vol. 113, no. 25, p. 257401, 2014.
[17] E. N. Bulgakov and A. F. Sadreev, ''Bloch bound states in the radiation continuum in a periodic array of dielectric rods,'' *Phys. Rev. A*, vol. 90, no. 5, p. 053801, 2014.
[18] J. Gomis-Bresco, D. Artigas, and L. Torner, ''Anisotropy-induced photonic bound states in the continuum,'' *Nat. Photonics*, vol. 11, no. 4, pp. 232–236, 2017.
[19] E. N. Bulgakov and D. N. Maksimov, ''Optical response induced by bound states in the continuum in arrays of dielectric spheres,'' *J. Opt. Soc. Am. B*, vol. 35, no. 10, pp. 2443–2452, 2018.
[20] K. Koshelev, A. Bogdanov, and Y. Kivshar, ''Meta-optics and bound states in the continuum,'' *Sci. Bull.*, vol. 64, no. 12, pp. 836–842, 2019.
[21] V. Mocella and S. Romano, ''Giant field enhancement in photonic resonant lattices,'' *Phys. Rev. B: Condens. Matter Mater. Phys.*, vol. 92, nos 1–5, pp. 1–5, 2015,
[22] E. De Tommasi, E. Esposito, S. Romano, et al., ''Frontiers of light manipulation in natural, metallic, and dielectric nanostructures,'' *Riv. Nuovo Cimento*, vol. 44, pp. 1–68, 2021.
[23] G. Zito, S. Romano, S. Cabrini, et al., ''Observation of spin-polarized directive coupling of light at bound states in the continuum,'' *Optica*, vol. 6, no. 10, pp. 1305–1312, 2019.
[24] J. Jin, X. Yin, L. Ni, M. Soljačić, B. Zhen, and C. Peng, ''Topologically enabled ultrahigh-Q guided resonances robust to out-of-plane scattering,'' *Nature*, vol. 574, no. 7779, pp. 501–504, 2019.
[25] S. Romano, G. Zito, S. Managò, et al., ''Surface-enhanced Raman and fluorescence spectroscopy with an all-dielectric metasurface,'' *J. Phys. Chem.*, vol. 122, no. 34, pp. 19738–19745, 2018.
[26] S. Arnold, M. Khoshsima, I. Teraoka, S. Holler, and F. Vollmer, ''Shift of whispering-gallery modes in microspheres by protein adsorption,'' *Opt. Lett.*, vol. 28, no. 4, pp. 272–274, 2003.
[27] S. Arnold, R. Ramjit, D. Keng, V. Kolchenko, and I. Teraoka, ''Microparticle photophysics illuminates viral bio-sensing,'' *Faraday Discuss*, vol. 137, pp. 65–83, 2008.
[28] Y.-n. Zhang, Y. Zhao, and R.-q. Lv, ''A review for optical sensors based on photonic crystal cavities,'' *Sens. Actuators, A*, vol. 233, pp. 374–389, 2015.
[29] C. Avitabile, L. Moggio, L. D. D'Andrea, C. Pedone, and A. Romanelli, ''Development of an efficient and low-cost protocol for the manual pna synthesis by fmoc chemistry,'' *Tetrahedron Lett.*, vol. 51, no. 29, pp. 3716–3718, 2010.
[30] L. M. Hellman and M. G. Fried, ''Electrophoretic mobility shift assay (EMSA) for detecting protein–nucleic acid interactions,'' *Nat. Protoc.*, vol. 2, no. 8, pp. 1849–1861, 2007.
[31] N. Bernhardt, K. Koshelev, S. J. White, et al., ''Quasi-BIC resonant enhancement of second-harmonic generation in WS_2 monolayers,'' *Nano Lett.*, vol. 20, no. 7, pp. 5309–5314, 2020.
[32] G. Zito, G. Rusciano, and A. Sasso, ''Enhancement factor statistics of surface enhanced Raman scattering in multiscale heterostructures of nanoparticles,'' *J. Chem. Phys.*, vol. 145, no. 5, p. 054708, 2016.
[33] G. Zito, G. Rusciano, and A. Sasso, ''Dark spots along slowly scaling chains of plasmonic nanoparticles,'' *Opt. Express*, vol. 24, no. 12, pp. 13584–13589, 2016.